SINGLE–CELL TRANSCRIPTIONAL AND EPIGENETIC MAPPING REVEALS CELLULAR AND MOLECULAR MECHANISMS DRIVING NON-ISCHEMIC CARDIAC FIBROSIS

Crisdion Krstevski[1,2,3], Gabriella E. Farrugia[1,2,3,] Ian Hsu[1], Malathi S. I. Dona[1,2], Taylah L. Gaynor[1,2,3], Charles D. Cohen[1,3], Rebecca L. Harper[1,3], Thomas I. Harrison[1], Bethany Claridge[1], Auriane Drack[1,4], Patrick Lelliott[1,3,4], Helen Kiriazis[4,5, 7], Aascha Brown [5], Julie R. McMullen[1,2, 4, 7], Daniel G. Donner[4,5, 7], Sean Lal[6], David W. Greening[1,2,3], Alexander R. Pinto[1,2,3,4,†]

[1]Baker Heart and Diabetes Research Institute, Melbourne, Victoria, Australia
[2]School of Agriculture, Biomedicine and Environment, Baker Department of Cardiovascular Research, Translation and Implementation, La Trobe University, Melbourne, Victoria, Australia
[3]Centre for Cardiovascular Biology and Disease Research, La Trobe University, VIC, Australia
[4]Baker Department of Cardiometabolic Health, University of Melbourne, Parkville VIC, Australia
[5]Preclinical Cardiology, Microsurgery and Imaging Platform, Baker Heart and Diabetes Institute, Prahran, VIC, Australia
[6]School of Medical Sciences, Faculty of Medicine and Health, University of Sydney and Department of Cardiology, Royal Prince Alfred Hospital
[7]Monash Alfred Baker Centre for Cardiovascular Research, Monash University, Melbourne, Victoria, Australia

†Corresponding author
alex.pinto@baker.edu.au

ABSTRACT

Cardiac fibrosis is a major cause of cardiac dysfunction. Recently, single-cell genomic approaches have revealed in unprecedented resolution the orchestrated cellular responses driving cardiac fibrosis. Yet, the fibrosis-causing phenotypes that emerge in the heart following non-ischemic cardiac stress, and the transcriptional circuits that govern cell identity and drive fibrosis, are not well understood. Applying a paired multiomic approach, we reveal key transcriptional circuits, in mouse and human hearts, which are associated with fibrosis development following non-ischemic cardiac insults, independent of disease model, species or biological sex. Strikingly, we find the key regulatory events driving fibrosis are reversible at the single-cell transcriptional and epigenomic level, further pointing to key factors regulating fibrosis development and resolution. The transcriptional regulators identified in this study represent promising targets to ameliorate the development of fibrosis in the context of chronic stressors such as aging and hypertension.

INTRODUCTION

Cardiac fibrosis—the excess deposition of extracellular matrix (ECM)—can lead to heart dysfunction and failure. Fibrosis accompanies many cardiovascular insults. These include ischemic insults such as myocardial infarction (MI), or in non-ischemic insults, such as systemic hypertension, where an expansion of interstitial and perivascular ECM occurs[1]. Determining the cellular and molecular drivers of fibrosis is critical for the development of clinical approaches for ameliorating the deleterious effects of fibrosis in different contexts.

We have only recently begun to understand with precision the diverse cell types that form the heart, including those that contribute to fibrosis. A catalyst for the rapid advance of this field has been the advent of single-cell genomics, which has enabled analysis of the cardiac cellulome—the integrated network of cells that form the heart—in high resolution[2–6]. This technology has made possible precise detection of cellular mediators of fibrosis[7–10], including 'activated' fibroblast subtypes that emerge following non-ischemic insults in both humans and mice, and are characterized by high expression of ECM-related genes[9,10]. Single-cell genomics has also been applied to decipher the gene regulatory networks (GRNs) that drive fibrosis and fibroblast activation. Given they act as nodes of control, GRNs may theoretically be therapeutically manipulated to ameliorate fibrosis development. However, our understanding, in particular their plasticity once exposed to fibrogenic stimuli such as hypertension, is rudimentary.

Here we have applied a paired multiomic approach—where both transcriptomic and epigenomic data is extracted from individual nuclei—to analyze cells from human hearts, and those from mice undergoing angiotensin II (AngII)-induced hypertension and cardiac remodeling. This unique dataset allowed us to gain new insights into transcriptional regulation in the context of cardiac fibrosis. Our analysis identified key transcription factors (TFs) that drive cell identity and non-ischemic fibrosis irrespective of species, disease model or biological sex. Further, we found fibrosis resulting from hypertension is reversible with significant plasticity evident in key GRNs that drive cardiac fibrosis. This work offers a resource for understanding the GRNs that govern cardiac cell identity and provides important insights of the cellular mediators and transcriptional circuity that drive fibrosis and heart failure.

RESULTS

Paired single-nucleus RNA-seq and ATAC-seq for the analysis of mouse cardiac tissue

To determine the core GRNs and corresponding TFs governing non-ischemic cardiac fibrosis, we initially used a hypertension-induced cardiac fibrosis model. To achieve this, we infused both male and female C57BL/6J adult mice (12-14 weeks of age) with AngII (1.4 mg/kg/day) or saline (control) for 14 days. Additionally, we tested the tractability and reversibility of GRN changes elicited by AngII infusion, by analyzing hearts from mice that underwent 14 days of AngII infusion followed by a 14-day recovery period (AngII+Rec), where ectopic AngII infusion was halted (Figure 1A).

Before examining cardiac changes induced by AngII we characterized the ability of our system to understand gene regulators that drive fibrogenic phenotypes. We sought to develop a pipeline that considers both transcriptome and enhancer elements to identify GRNs that drive phenotypes of disparate cardiac cell types. Therefore, we performed parallel high-throughput profiling of transcriptomes and chromatin accessibility of individual nuclei of cardiac cells, using single-nucleus RNA sequencing (snRNA-seq) and single-nucleus Assay for Transposase-Accessible Chromatin sequencing (snATAC-seq) (Figure 1A, see Methods). Our paired analysis yielded a total of 22,182 nuclei that passed quality control measures (Supplementary Figure 1), where high-quality transcriptomic and genomic data could be retrieved, averaging a total of ~7,231 nuclei per sample with a median number of 229,746 ATAC-seq fragments and 32,285 RNA-seq reads per nucleus. Dimensionality reduction and clustering of cells enabled classification of cell types based on paired transcriptomic and ATAC read outs (Figure 1B). We noted cell types could also be distinguished based on either transcriptomic (Figure 1B and 1C; Supplementary Figure 2A) or chromatin accessibility data alone (Figure 1B and 1D). Quantification of cells corresponding to individual timepoints showed relatively uniform contributions of cells from each sample (Supplementary Figure 1A-B).

Our dataset included all major cardiac cell types marked by distinct features. These include cell-type specific enrichment of transcripts, with those corresponding to key marker genes such as: *Ttn*, *Myh6* for CMs; *Dach1*, *Cyyr1*, *Flt1* for endothelial cells (ECs); *Npr3*, *Vwf* for endocardial cells; *Pcdh9*, *Tnxb* for fibroblasts; *F13a1, CD74* for macrophages; Abcc*9, Rgs5* for pericytes; *Myh11*, *Acta2* for smooth muscle cells (SMCs) (Figure 1C). Our dataset also captured extensive substructure within individual cell populations, with cell-specific transcriptional patterns within these cell subsets (Supplementary Figure 2B). Our snATAC-seq data showed cell-specific patterns of reads corresponding to genetic loci (Figure 1D). While open chromatin measures generally followed well-established patterns of cell-specific gene activity (Figure 1D), our findings complicate the capacity to use snATAC-seq alone to infer gene activity. For example, we note *Tcf21* gene locus is accessible in fibroblasts and mural cells (pericytes and SMCs; Figure 1D), despite *Tcf21* gene expression being restricted to cardiac fibroblasts[11]. This identifies a challenge for inferring gene activity using chromatin accessibility alone and highlights the value of accompanying paired transcriptomic data.

To determine GRNs underlying cell-type-specific phenotypes, we inferred transcriptional regulators using the SCENIC+ pipeline[12]. SCENIC+ leverages both epigenomic and transcriptomic data to infer enhancer-driven regulons (eRegulons)—genetic modules of TFs and their target genes. These are identified for each cell population using snATAC-seq data to determine enhancer accessibility and snRNA-seq data to determine TF and putative TF target gene expression. Correspondingly, this approach generates enhancer-driven GRNs (eGRNs). Using this pipeline, top distinct regulons identified for each cell type (Figure 1E) included those previously associated with specific cell types, such as Gata4, Ppara, Esrrg for CMs; Sox7, Foxp1 and Erg for endocardial cells; Fli1, and Ets1/2 for ECs; Sox9 and Pdgfra for fibroblasts; and Maf, Mafb, Spi1 and Runx1 for macrophages.

To verify cell-specific characteristics driving eRegulon discovery, we were able to assess features enabling cell-specific TF activity. Using Ppara and Sox9 (Figure 1F-G, respectively), for example, cell-type-specific eRegulon enrichment also accompanied enrichment of mRNA and accessibility of DNA binding sites for the respective TF. Further, immunostaining validated expression findings showing high PPARa (Figure 1F) in myocytes and SOX9 (Figure 1G, Supplementary Figure 5) in non-myocytes. However, our analyses also shows that neither TF gene expression nor the accessibility of the DNA binding sites for the TF alone are sufficient to yield transcription factor activity (Figure 1F-G). Therefore, while our pipeline enables discovery of TF activity, it also underscores the value of paired transcriptomic and epigenetic analysis for identifying TF activity governing cell identity.

Paired single-nucleus RNA-seq and ATAC-seq analysis of human cardiac tissue

Next, we sought to determine if a similar paired multiomic approach could be applied to identify core GRNs driving diverse cellular phenotypes in the human heart. To achieve this, we mechanically dissociated cardiac samples from pre-mortem donor hearts from four females and four males with no clinical record of heart failure, extracted and sorted nuclei, and performed paired snRNA-seq and snATAC-seq (Figure 2A; see Methods). Our pipeline yielded 11,097 nuclei passing quality control criteria for transcriptomic and epigenomic data, representing major cardiac cell populations (Figure 2C; Supplementary Figure 3). Similar to our mouse dataset (Figure 1), human cardiac cell populations could be segregated based on snRNA-seq or snATAC-seq data. High enrichment of established cell-type-specific genes transcripts confirmed cell type identity (Figure 2D; Supplementary Figure 4). These included TTN, MYH6 for CMs, NEGR1 for fibroblasts; VWF for ECs, CD163, STAB1 for macrophages and MYH11 and CARMN for SMCs (Figure 2D). Again, we noted a substructure within individual cell types, most notably in CMs (Supplementary Figure 4B). Interestingly, while deconvolution of individual human samples contributing to the dataset revealed that non-myocyte cell subsets were composed of cells from all 8 individual donor samples, CM subsets mostly segregated based on individual donors (Supplementary Figure 4C). Examination of accessible chromatin also revealed cell-type specific patterns. These included MYH6 for CMs; DNMT1 for fibroblasts; FLT1 for ECs; CARMN for SMCs; PDGFRB for pericytes and C1QB for macrophages (Figure 2E). Finally, based on both snRNA-seq and snATAC-seq data, we identified eRegulons enriched within human cardiac cell types. These include GATA4 and PPARA in CMs, validated histologically (Supplementary Figure 5), and FLT1 in ECs, and SPI1 and EBF1 in macrophages (Figure 2F-E, Supplementary Table 1).

Together, recovery of well-established master regulators of key cardiac cell types by our eGRN analysis of mouse and human hearts, demonstrate the advantages of applying a paired multiomic approach for discovering key transcriptional circuits governing cellular phenotypes.

Multiomic analysis reveals gene regulatory network dynamics in non-ischemic fibrosis

Encouraged by our results, we applied this approach to determine core GRNs that drive development of cardiac fibrosis using the AngII-induced hypertension model. Picrosirius red (PSR) staining for collagen showed extensive cardiac fibrosis in response to hypertension in males and females (Figure 3A-B), with corresponding changes in a range of physiological parameters including systemic blood pressure (BP) (Supplementary Figure 6). Analysis of differentially expressed genes ($p<0.01$) between matching cell populations from Saline and AngII mice, showed significant changes in gene expression in cardiac cells (Figure 3C). Gene Ontology (GO) enrichment analysis mirrored cardiac fibrosis determined by histology, with genes induced by AngII corresponding to GO terms associated with ECM remodeling and transforming growth factor β (TGFβ) signaling, particularly by fibroblasts (Figure 3D). These included genes such as *Cilp*, *Col3a1* and *Jun*, associated with TGFβ response in fibroblasts, or *Postn*, *Col8a1, and Cnn2* associated with ECM remodeling (Supplementary Table 2). Among the top down-regulated pathways in CMs were those related to cardiac contraction. These included genes such

as *Gsn*, *Pde4d* and *Tpm1*. CMs also had several genes related to oxidative stress response downregulated, including *Map3k5*, *Cd36* and *Fos* (Figure 3D, Supplementary Table 2).

To determine the GRNs driving fibrogenic phenotypes, we compared enrichment of eRegulons across major cell populations of Saline and AngII mouse hearts (Figure 3E-F). Among the top eRegulons differentially enriched between the two conditions were those such as Smad3, a key mediator of TGFβ signaling, Egr3, Nfkb1, and Nfatc2, all implicated in fibrosis[13–15]; (Figure 3E). Also, among enriched eRegulons were those that are less recognized in cardiac fibrosis such as Creb3l2, and Etv6. eRegulons with the most marked reduction in enrichment included androgen receptor (Ar), Cebpd, *Krüppel-like factor* (KLF) family members (including Klf2, 4, 6 and 9), *Jun* family members (Jun, Junb, Jund) and Tcf21. Many of these, including Cebpd and Klf4, have been independently demonstrated to be down-regulated upon AngII stimulation of the heart and other models of fibrosis [16,17]. Finally, evaluation of potential sex-specific GRNs showed the majority of eRegulons were present in both sexes (Figure 3G).

***Elevated Cilp* and *Thbs4* expression define fibrogenic fibroblasts in mouse and human non-ischemic cardiac fibrosis**

Analysis of AngII-treated mouse hearts revealed an increase in proportion of a fibroblast population enriched for fibrosis-related gene transcripts. As identified in our previous study [10], we found these cells highly enriched for *Cilp* and *Thbs4* transcripts (Figure 4). Here, we collectively refer to these cells as 'Fibro-*Cilp*', and as previously reported[10], were able to determine their presence in regions of fibrosis within hearts of AngII-treated mice (Figure 4A-C and Supplementary Figure 7). These cells are present in both female and male contexts[10]. To evaluate *Cilp* and *Thsbs4* as markers of fibrogenic cells in a different model of non-ischemic fibrosis, we examined data from mice 18 days after thoracic aorta constriction (TAC)[18]. Similar to our AngII model, fibrogenic cells of this model were highly enriched for *Thbs4* and *Cilp* transcripts, with THBS4 detectable within fibrotic regions of TAC mouse hearts[19] (Figure 4D-F and Supplementary Figure 8). We next determined whether Fibro-*Cilp* cells were present within the dataset prepared by multiomic analysis of the human heart (Figure 2). Here we noted fibroblasts were comprised of two cell subsets: one subset that is highly enriched for fibrogenic gene signatures and another that is not (Figure 4G-H). Corresponding to our analysis of AngII and TAC mouse datasets, we found that fibrogenic cells in our human dataset are enriched for CILP and THBS4 transcripts (Figure 4G-H and Supplementary Figures 9 and 10), with THBS4 detectable within the human heart tissue (Figure 4I and Supplementary Figure 10C). Consistent with these findings, we also found high enrichment of THBS4 transcript within remote fibrosis regions of human hearts following MI, determined using a dataset from an unaffiliated study[20] (Figure 4J). Together our analysis reveals a common fibrogenic cell type that emerges in the context of non-ischemic fibrosis, irrespective of species or biological sex.

Multi-model and multiomic single-cell analyses identify core TFs shaping Fibro-*Cilp* phenotype

Next, we focused on identifying the gene regulatory circuits driving Fibro-*Cilp* phenotype. To do this, we initially compared Fibro-*Cilp* to other fibroblasts from AngII mouse hearts. As noted previously (Figure 4), we found high enrichment of transcripts corresponding to genes linked to fibrosis within Fibro-*Cilp* cells. These included those forming a fibrosis signature ('fibrosis signature' genes: *Col1a1, Col3a1, Col8a1, Postn,* and *Tnc*) in addition to other genes including *Eln* and *Piezo2* (Figure 5A-B; Supplementary Table 3). Accordingly, top GO terms representing genes enriched in Fibro-*Cilp* included those associated with ECM (Figure 5C).

To assess the generalizability of the Fibro-*Cilp* phenotype, we drew on combined data from this study, our previous scRNA-seq study of AngII-induced fibrosis[10], TAC mouse hearts[21] (Figure 5D). Differential gene expression analysis ($p<0.01$) comparing Fibro-*Cilp* to other fibroblasts confirmed similar features of Fibro-*Cilp* cells from different non-ischemic contexts. There was high level of overlap between Fibro-*Cilp*-enriched gene sets from AngII and TAC-stressed heart scRNA-seq datasets

(Figure 5E). There was markedly less overlap between Fibro-*Cilp*-enriched genes from scRNA-seq and snRNA-seq datasets from AngII-treated mouse hearts, reflecting the reduced number of genes captured by the snRNA-seq approach. However, we identified 32 genes—including fibrosis-linked matricellular genes *Postn, Cilp, Thbs4, Ddah2, Sparc* (Supplementary Table 4)—that are highly enriched in Fibro-*Cilp* cells in all four contexts. GO enrichment analysis showed these were primarily linked to ECM- and fibrosis-related programs (Figure 5E).

Next, we leveraged the human and mouse multiomic datasets to identify eRegulons that are highly enriched in Fibro-*Cilp* cells compared to other fibroblasts across both species. Our analysis found 30 common TFs more active in Fibro-*Cilp*, including many TFs that have been recently associated with fibrosis (Figure 5F; Supplementary Table 4). These included MEOX1[18], TEAD1[9], RUNX1[22,23] amongst others. We also discovered many TFs that have not—to the best of our knowledge—been associated with fibrosis. GO enrichment analysis of these identified the disparate functions these TFs participate in, with many top statistically significant terms linked to tissue development or differentiation (Figure 5F)

We also found genes comprising eRegulons varied, indicative of the different aspects of the Fibro-*Cilp* phenotype they regulate. While the numbers of genes linked to a TF is a function of statistical parameters applied to undertake eRegulon discovery[12], the largest eRegulons discovered by our analysis of AngII hearts were Nfia, Nfib, and Tcf12, associated with 1807, 1428 and 1214 genes, respectively (Figure 5G). To infer the potential role of TFs in establishing the Fibro-*Cilp* phenotype, we performed GO enrichment analysis on genes constituting eRegulons. Consistent with many genes up-regulated in fibroblasts being linked to TGFβ responses (Figure 5C), 47% of TFs had statistically significant enrichment of genes linked to the *response to TGFβ* GO term. Further, many TF-linked genes were involved with terms linked to ECM remodeling, with some linked to cardiac hypertrophy (Figure 5G).

To study potential sex differences, we determined eRegulons that distinguish Fibro-*Cilp* from fibroblasts from AngII-treated female and male mice separately (Figure 5H). We found most Fibro-*Cilp*-enriched eRegulons in female mouse hearts were those enriched in Fibro-*Cilp* cells in male hearts, while we found more that were unique to males, based on our statistical parameters (Figure 5H). Nevertheless, we identified 95 TFs that are highly active in Fibro-*Cilp* cells in both sexes with these corresponding gene programs linked to ECM remodeling such as '*connective tissue development*', '*osteoblast differentiation*' and '*ossification*'. Together, our analyses have identified core TFs that drive Fibro-*Cilp*'s phenotype irrespective of species, biological sex or model of non-ischemic fibrosis.

Reverse cardiac remodeling identifies transcription factors driving reversible non-ischemic fibrosis

Next, we sought to determine the plasticity and elasticity of GRNs driving cardiac fibrosis. To achieve this, we analyzed hearts of AngII and AngII+Rec mice (Figure 1A). We found withdrawal of AngII infusion led to reduction of fibrosis—determined by PSR staining of tissue and subsequent quantification (Figure 6A)— associated with cessation of AngII-induced hypertension (Supplementary Figure 11). Further examination of gene expression in fibroblasts of AngII+Rec compared to AngII mice showed downregulation of several fibrosis-associated genes including those encoding ECM components and key matricular protein genes such as *Postn*, *Cilp,* and *Thbs4* (Figure 6B). Consistent with a reduction Fibro-*Cilp* marker gene transcripts (*Cilp* and *Thbs4*), importantly, we found a reduction of this fibroblast subset within total cardiac fibroblasts. This was independent of sex, and resulted in AngII+Rec Fibro-*Cilp* cells reaching levels comparable to Saline mice (Figure 6C). Finally, reduction of Fibro-*Cilp* cells and *Thbs4* gene expression was validated by immunostaining which confirmed reduced fibrotic regions and THBS4 within hearts after recovery from AngII infusion (Figure 6D-E).

To determine the extent to which the fibrosis-inducing gene signature is reversed, we compared genes upregulated in AngII (AngII vs Saline) and then downregulated in recovery (AngII+Rec vs AngII) in

major cardiac cell types. GO enrichment analysis revealed multiple processes associated with ECM and fibrosis (Figure 6F) reversibly induced in fibroblasts, ECs and macrophages. Further, top reversibly induced genes in CMs correlated with processes involved in ECM signaling/interaction or those involved in myocyte structure (Figure 6F).

Next, we examined whether the reversal of fibrosis in AngII+Rec mice corresponds to a reversal of fibrosis-inducing TF activity. Comparison of eRegulon enrichment in AngII and AngII+Rec cell types revealed induction or repression of TF activity consistent with recovery from fibrosis. The activity of fibrogenic TFs induced by AngII such as Smad3—reflecting TGFβ signaling—Frem1, Creb3l2, Meox1, Pknox and others showed corresponding down regulation in AngII-Rec (Figure 6G-H, Supplementary Figure 13 and 14). In contrast, many TF activities suppressed by AngII-infusion were increased in AngII+Rec cardiac cells. These included Cebpd, Jund, and Klf4 (Figure 6G-H, Supplementary Figure 14). Other TFs departed from this pattern, for example Id2—associated with repression of TGFβ signaling and fibrosis[24]—was absent from our list of top TFs suppressed by AngII, but was induced in AngII+Rec cells.

Finally, we compared changes in TF activity in fibroblasts of each sex after removal of AngII. Major TFs largely overlapped between sexes, and these common TFs corresponded to GO terms associated with ECM such as *ossification* and *connective tissue development* (Figure 6I, Supplementary Figure 12). These observations suggest core TFs governing fibrosis and its reversal are independent of sex.

Validation of distinct roles of TFs in regulating fibroblast phenotype and ECM deposition

To validate the role of core TFs identified in the context of TGFβ signaling, we tested the impact of TF gene silencing on the proteome landscape of primary human ventricular fibroblasts treated with TGFβ (Figure 7, Supplementary Figure 15). TGFβ treatment is a well-established model of fibroblasts-myofibroblast differentiation. Although myofibroblasts are absent in the setting of fibrosis we have examined here, we chose this system because fibroblasts exhibit a TGFβ response gene signature in non-ischemic fibrosis (Figure 3).

Treatment of cells with TGFβ, or TGFβ and siRNA corresponding to TFs, altered the proteomic landscape of fibroblasts (Figure 7B). Changes in several key protein expression patterns after TGFβ treatment were consistent with those anticipated based on transcriptional activity of fibroblasts in non-ischemic fibrosis. TGFβ-treatment elevated levels of CCN2, COL1A1 and COL5A2, and others, including those implicated in myofibroblast differentiation or fibrosis, while ECM-related proteins such as COL3A1—which are reduced in expression non-ischemic fibrosis—were also lower after TGFβ-treatment (Figure 7C). However, our proteomic profiling also found expression of hallmarks of non-ischemic fibrosis, such as COL8A1 and POSTN (Figure 7D), were reduced or unchanged following TGFβ treatment (Figure 7B, Supplementary Table 7). Therefore, *in vitro* assays, particularly those leading to myofibroblast differentiation, do not precisely recapitulate phenotypes observed in non-ischemic fibrosis *in vivo*.

Nevertheless, silencing of TFs revealed their distinct roles in regulating fibroblast phenotypes and ECM network (Figure 7C-D, Supplementary Table 7). For example, silencing CREB3L2, NFAT5, RCOR1 RUNX1 and NFIB all resulted in reduced levels of COL5A1 in response to TGFβ-treatment compared to unsilenced controls (Figure 7D). Distinct patterns of TF involvement were also found for other key ECM components such as COL1A1, COL3A1, COL5A2 and COL6A1. Similarly, TFs tested were important for expression of matricellular proteins, including CTHRC, TGFBI, TNC, and VCAN. CREB3L2 was a common, key regulator found to be important for expression of most of these genes. We also found evidence of potential gene repressive activities of TFs. For example, NFIB and RUNX1 silencing lead to a marked increase in COL3A1 protein levels, comparable to non-TGFβ treated controls (Figure 7D, Supplementary Table 7), while BNC2 and NFAT2 silencing had the opposite effect (Figure

7D). Together, these observations demonstrate the different roles that TFs play in fibroblast phenotypes and ECM deposition, and their complex roles in driving non-ischemic fibrosis.

DISCUSSION

Fibrosis is a major contributor to cardiac dysfunction resulting in heart failure. Using mouse models, human heart tissue and leveraging single-cell transcriptomics and epigenomics, we aimed to gain a more comprehensive understanding of the GRNs driving cardiac cell identity and fibrogenic phenotypes. Our study has yielded new insights regarding the genetic circuits that are driving cell-specific and non-specific mechanisms of non-ischemic fibrosis.

A key feature of our study is the application of a paired multiomic approach—combining both snRNA-seq and snATAC-seq—to uncover transcriptional regulators of fibrosis development. While others have integrated these technologies using unpaired pipelines, where snRNA-seq and snATAC-seq libraries are prepared from separate pools of cells, in our approach transcripts and open chromatin fragments are extracted from the same nuclei for each cell. The paired approach overcomes challenges posed by integrating separate datasets, which relies on assumptions and data transformations such as converting snATAC-seq data to gene expression level. This may include the erroneous inference that a gene is active in a cell solely based on chromatin accessibility. These assumptions overly simplify the complex mechanisms underlying transcriptional regulation, and this is clearly demonstrated in our data. For example, snATAC-seq indicates the genetic locus of *Tcf21* is open in fibroblasts, SMCs and pericytes, despite *Tcf21* transcript being present only in fibroblasts. Using *Ppara* and *Sox9* as examples, our analyses also show that transcriptional activity (based on expression of target genes) does not always correlate with TF transcript level or chromatin accessibility of corresponding DNA-binding motifs. Armed with this unique dataset we calculated the major GRNs of single cells in different contexts and applied this to understand cellular diversity and drivers of fibrosis in different cardiac contexts.

A key application of single cell omics data is the classification of cell populations and subtypes based on distinct transcriptional signatures. GRNs identified in our analyses included TFs with well-established roles in cardiac cell development such as Nkx2-5, Fli1, Tcf21, Spi1, that are active in CMs, ECs, fibroblasts and macrophages, respectively, confirming the validity of our approach for the classification of major cardiac cell types. We were also able to recover TFs in a cell-specific manner from human data.

A major outcome of our analysis was the determination of key TFs that drive non-ischemic cardiac fibrosis. Most TFs exhibiting altered activity following AngII treatment operated in multiple cell-types. Shown here and previously[10], virtually all cardiac cell types contributed to ECM remodeling with gene programs associated with TGFβ signaling. Reflecting this, Smad3—a key mediator of TGFβ signaling—was activated in multiple cell types. We also recovered a multitude of TFs that have been implicated in fibrosis including Nfkb1[15], Bnc2[25], Meox1[21] and Egr3[13]. Further, we identified TFs with reduced activity upon development of fibrosis. These included JunD, Cebpd, Id2 and Klf4, all of which have been negatively correlated or implicated in dampening development of fibrosis[16,17,24,26,27]. Alongside TFs known to be involved in fibrosis our study uncovered several less-well associated, or previously unlinked, to cardiac fibrosis such as Creb3l2, Nfic and Phf20. Systematic exploration of these TFs will be required in the future to determine their role in the development of fibrosis.

Our analysis also provides a more comprehensive understanding of the highly fibrogenic cell population, Fibro-*Cilp*, that emerges in non-ischemic cardiac fibrosis. This population comprises both Fibroblast-*Cilp* and Fibroblast-*Thbs4* subsets we and others have recently identified[10,28].

The generalized signature of Fibro-*Cilp* cells, independent of disease model, species or biological sex, is characterized by high expression of ECM structural genes and matricellular proteins. Although there were context dependent differences in these cells, GRN analysis identified a core set of TFs that regulated different aspects of Fibro-*Cilp* phenotypes. These included Meox1, Tead1, Runx1, and others which were recently identified as transcriptional regulators of 'activated' fibroblasts in single-cell genomic studies examining pressure-overloaded heart models[9,18] or in the context of human cardiac

remodeling[23]. Others we identified, such as Foxo1, have been demonstrated to regulate myofibroblast differentiation *in vitro* or *in vivo* following MI[29,30]. Using high-throughput proteomics, we were able to validate the roles of many of these in regulating human cardiac fibroblast ECM production *in vitro.*

We extended our exploration of key TFs driving fibrosis to cardiac recovery. Reverse remodeling of the heart has been noted in studies examining the impact of AngII or AngII receptor inhibitors, such as angiotensin II type 1 (AT_1) blockers[31], or murine pressure overload studies where bands constricting aortae or pulmonary arteries inducing cardiac hypertrophy are removed[32,33]. These studies demonstrate that both fibrosis and hypertrophy of the heart have the capacity for reversion to baseline levels. Here we confirm these findings showing that a key feature of reverse remodeling elicited by AngII withdrawal is the elimination of fibrosis, which occurs regardless of sex.

More recently, reverse remodeling has been explored using single-cell genomics. Alexanian and colleagues[21] showed *bromodomain and extra-terminal domain* (BET) inhibitor JQ1 reverses pressure overload-induced cardiac remodeling. In this model *Meox1* is a key mediator of fibroblast activation that is downregulated upon JQ1 triggered recovery. Consistent with this, our analysis shows *Meox1* activation under AngII treatment and subsequent downregulation during recovery. Although we found that *Meox1* was not only important for fibroblast activation. *Meox1* was present in fibroblast populations enriched for *Wif1*[3,34,35], in non-stressed hearts and a range of cell types—including macrophages, ECs, endocardial cells, and to a lesser degree, CMs—following AngII treatment. Another TF, *Runx1*, is implicated in reverse remodeling following LVAD implantation[36]. This too, we found, was reversibly activated in fibroblasts (and other cells), although it was not amongst the top significantly activated and deactivated TFs after AngII treatment and withdrawal (respectively) in our analysis. Among the top genes downregulated under AngII and increased in expression following withdrawal was Klf4, Cebpd and Id2, which are implicated in attenuating cardiac fibrosis[16,17,37]. KLF4 also controls other aspects of cell activity that may be related to controlling fibroblast phenotypes, including epigenetic programming[27]. Overall, our data helps tease-out the mechanisms and key TFs driving not just detrimental fibrosis but those driving recovery.

In this study we focused on transcriptional circuits driving fibrosis. We also restricted our consideration to activators of gene transcription rather than repressors. The[38] approach we have applied here, and our dataset, could be expanded to these. Findings could also be extended to the examination of other cardiac phenotypes aside from fibrosis, such as CM hypertrophy, as has been examined by others[38]. Sex-specific patterns of gene expression and corresponding GRNs were also beyond the scope of this study and will explored in subsequent studies by us and others.

Finally, there are several limitations of our study which may have restricted our ability to fully uncover TFs driving cell identity and fibrogenic responses. These include: low yield of reads from our transcriptomic and epigenomic libraries leading to reduced power to discover eRegulons; low numbers of cells of specific cell types; and heterogeneity of sampling sites of human cardiac tissue. Further, in all our data, the reduced capture of transcripts due to nuclei isolation and permeabilization protocols, may have reduced our capacity to discover and identify eRegulons, which are partly contingent on capturing reads corresponding to TFs[12].

In summary, by integrating data from multiple mouse models, human samples and leveraging single-cell multiomic methodologies, we have captured key TFs that drive cardiac fibrosis. In addition to identifying core transcriptional regulators that are well-implicated in cardiac fibrosis, we have also discovered a multitude of new TFs, involved both in induction and reversal of fibrosis. Collectively, this work provides exciting new avenues of research for informing clinical applications for reversing fibrosis and its deleterious effects.

Methods

All experimental procedures were performed on C57BL/6J mice following protocols approved by Alfred Research Alliance (ARA) Animal Ethics Committee (application number E/1990/2020/B). Human studies were approved by the Alfred Hospital Ethics Committee (application number 143/19). The Sydney Heart Bank at the University of Sydney has Human Research Ethics Approval 122/2021.

For detailed additional information see Supplementary Material.

Acknowledgements

The authors acknowledge use of the facilities at the Alfred Research Alliance Flowcore Cytometry Platform, the Monash Histology Platform, and the Baker Heart and Diabetes Institute Microscopy Platform. The authors acknowledge the Australian Red Cross for the historical coordination of the donor heart collections.

This work was funded by grants from the National Health and Medical Research Council (NHMRC; GNT1188503, GNT2021463) to A.R.P., and Australian Government Defense Science Institute RhD Student Grant to T.L.G.. Further, T.L.G., C.D.C., C.K., and G.E.F., were Supported by Australian Government Research Training Program stipends. A.R.P. is the recipient of the National Heart Foundation Australia, Future Leader Fellow, Level 3 (reference number 107335). D.W.G was supported by the National Heart Foundation Australia (reference number 105072) and by grants from the Medical Research Future Fund (MRFF; MRF1201805, MRF2024039). J.R.M was supported by a NHMRC Senior Research Fellowship (grant number 1078985) and Baker Fellowship (The Baker Foundation, Australia).

Figure 1

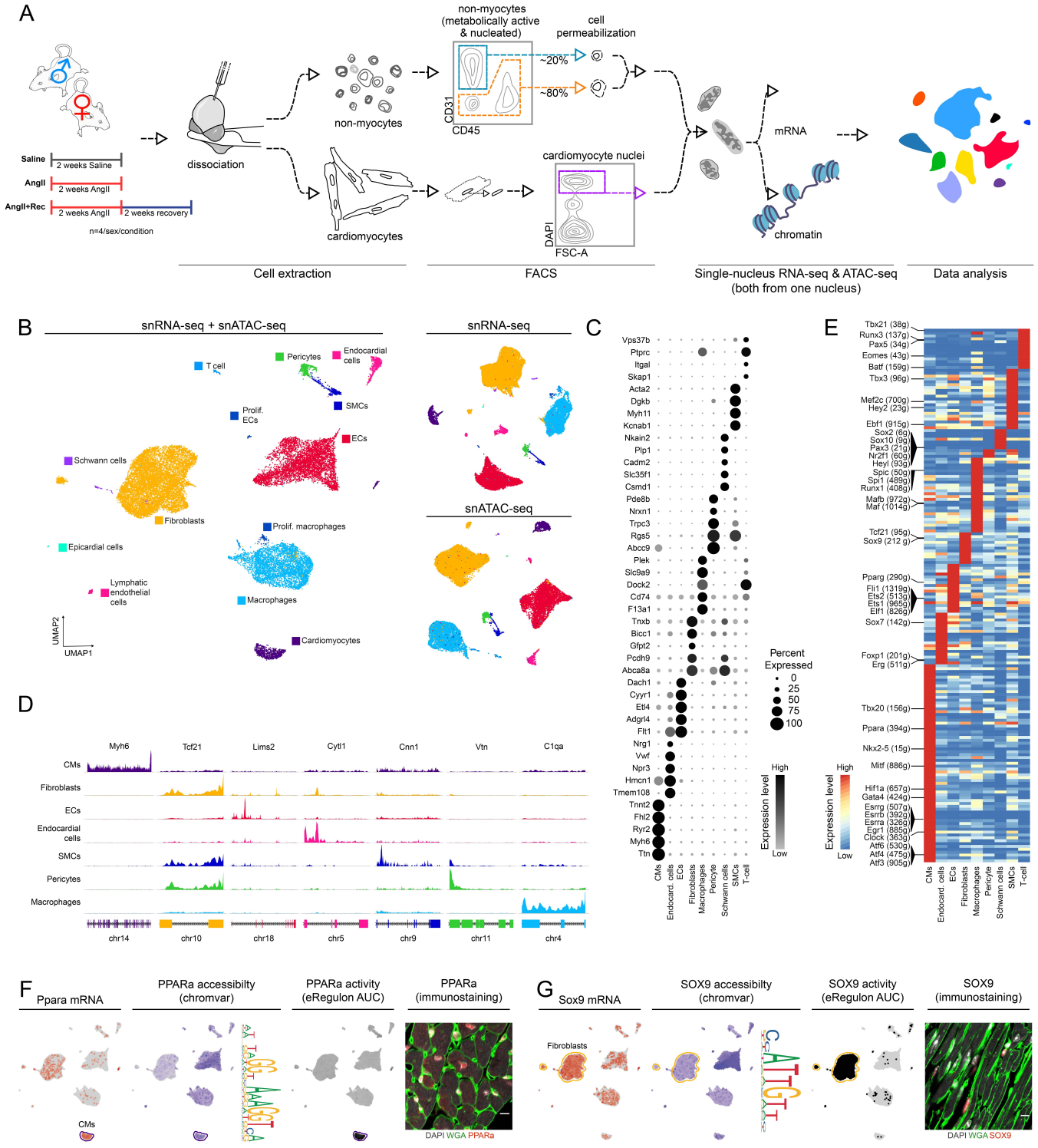

Figure 1. High-throughput single-cell transcriptomic and epigenomic profiling of the mouse heart.

A. Experimental pipeline for performing paired single-nucleus RNA-sequencing (snRNA-seq) and single-nuclear Assay for Transposase Accessible Chromatin (ATAC)-sequencing (snATAC-seq) using mouse heart with and without physiological stress. Left panel shows experiment cohorts used for mouse experiments: mice infused with saline or AngII for two weeks; or those infused with AngII for two weeks followed by an additional two weeks of recovery where ectopic AngII infusion was ceased.

B. Uniform manifold approximation and projection (UMAP) of combined scRNA-seq and snATAC-seq data (left panel), snRNA-seq data alone (top right panel) or snATAC-seq data alone (bottom right panel). Each plot shows 22,182 cells.

C. Top 5 distinct genes for each cell population determined by snRNA-seq. Dot size and intensity indicate cell proportion expressing the gene and relative gene expression level.

D. Aggregate accessibility profiles for selected genes with relative cell-specific expression. Chromosome location and exons corresponding to genes indicated at the bottom.

E. Enhancer-driven gene regulatory network (GRN) plot identifying core eRegulons enriched within cardiac cell populations determined using the SCENIC+ pipeline. The heat map depicts transcription factor (TF) expression of the eRegulon on the color scale. Number of TF target genes comprising the eRegulon indicated in parenthesis following the TF name.

F. UMAPs corresponding to transcript level (grey-red, low-high, respectively), chromatin accessibility depicted using Chromvar package (grey-purple, low-high, respectively; with accompanying sequence logo) and eRegulon activity (grey-black, low-high, respectively) for Ppara. Accompanying micrograph shows Ppara in cardiac cells. Scale bar indicates 100 μm.

G. Same as F, but for Sox9.

Figure 2

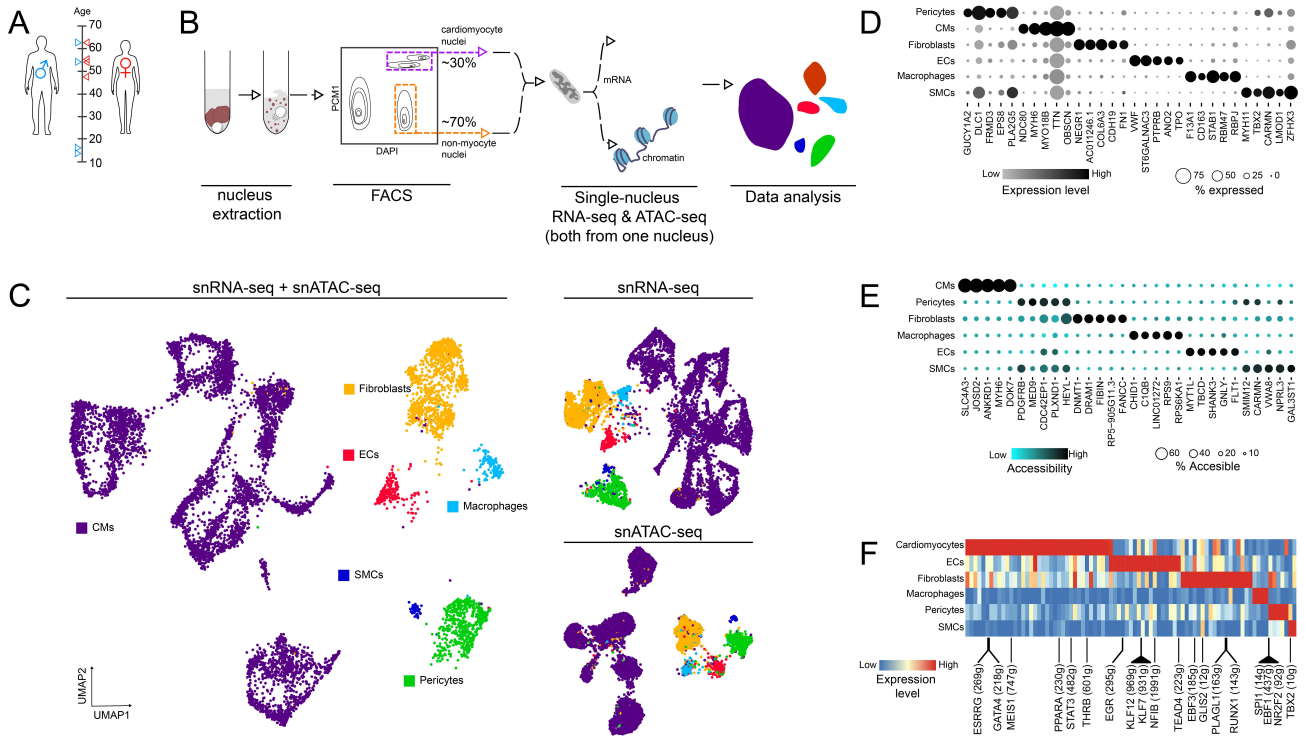

Figure 2. Overview of single-cell transcriptomic and epigenomic profiling human of heart tissue.

A. Gender, age and number of donor heart samples used for paired snRNA-seq and snATAC-seq.
B. Pipeline for performing paired snRNA-seq and snATAC-seq using human following mechanical tissue dissociation of donor heart tissue.
C. UMAP of combined scRNA-seq and snATAC-seq data (left panel), snRNA-seq data alone (top right panel) or snATAC-seq data alone (bottom right panel). Each plot shows 13,824 cells.
D. Top 5 distinct genes for each cell population determined by snRNA-seq. Dot size and intensity indicate cell proportion expressing the gene and relative gene expression level.
E. Genes associated with the top 5 accessible chromatin regions for each cell population determined by scATAC-seq.
F. GRN plot identifying core eRegulons enriched within cardiac cell populations determined using the SCENIC+ pipeline. The heat map depicts transcription factor (TF) expression of the eRegulon on the color scale. Number of TF target genes comprising the eRegulon indicated in parenthesis following the TF name.

Figure 3

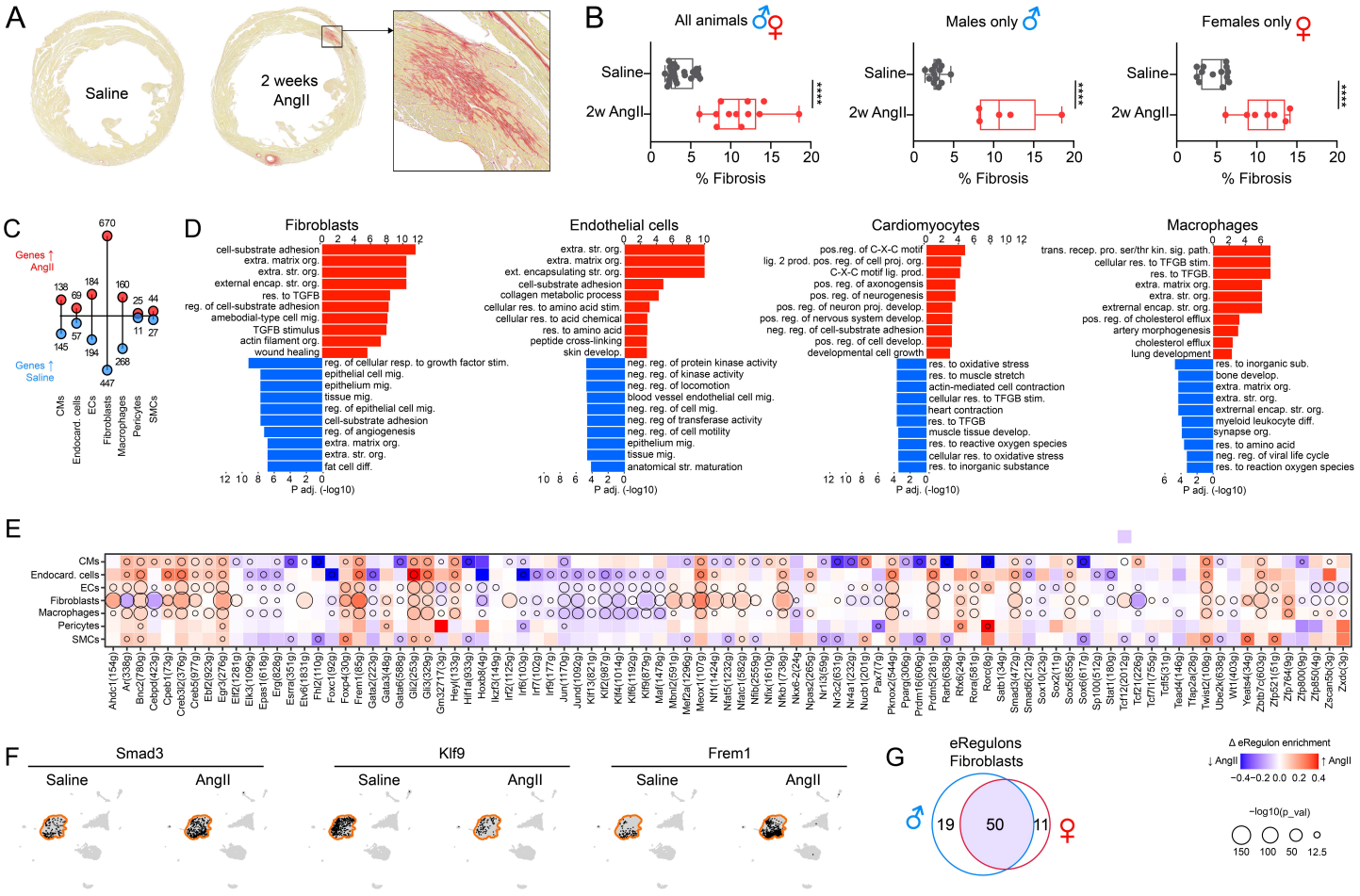

Figure 3. Determining the transcriptional regulation after AngII induced cardiac remodeling.

A. Representative micrographs of picrosirius red stained cardiac cross sections from Saline or AngII mice.

B. Change in cardiac fibrosis with and without induction of hypertension in both females and males (N= 5-6 animals per group). Cardiac fibrosis was measured from mid-ventricular sections. P-values on plot are derived from Wilcoxon test for differences in mean.

C. Gene expression changes in major cardiac cell populations. Lollipop plot summarizing number of upregulated (red)and downregulated (blue) genes ($p < 0.01$) in AngII mouse heart cells relative to Saline heart cells.

D. Gene Ontology (GO) enrichment analysis of genes that are up- and down-regulated in fibroblasts, ECs, CMs and macrophages.

E. Heatmap/dot plot summarizing changes in eRegulon enrichment in cardiac cells types between AngII and Saline mouse hearts. Heatmap color and intensity indicate direction and magnitude of change in eRegulon enrichment. Circle size indicates the statistical significance (Wilcoxon signed-rank test).

F. UMAPs displaying binarized eRegulons enrichment within fibroblasts (outlined). Smad3 and Frem1 were chosen as eRegulons that indicate activation of these TFs in AngII mouse cardiac fibroblasts. Klf9 was chosen as an example of a TF that is repressed in cardiac fibroblasts after AngII treatment.

G. Proportional Venn diagram of eRegulons that are more highly enriched in cardiac fibroblasts after AngII treatment in males and females.

Figure 4

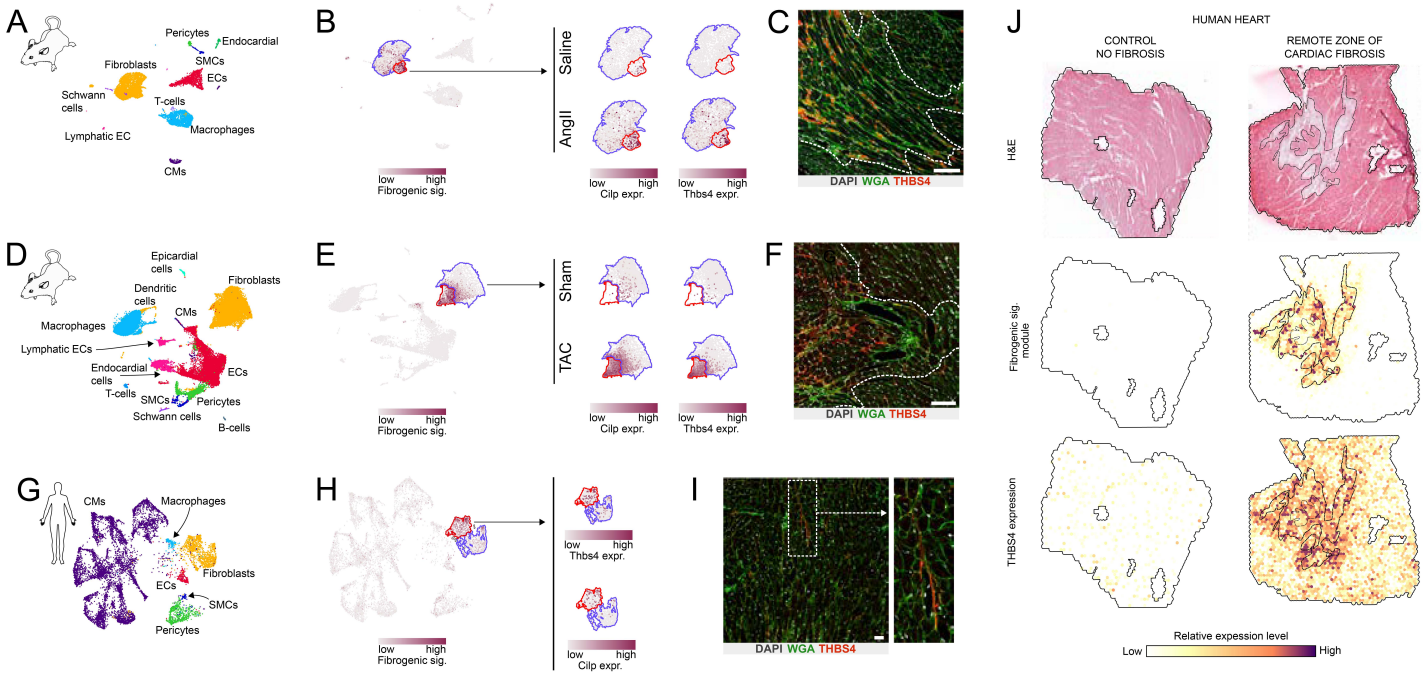

Figure 4. Fibro-Cilp cells are the primary fibrosis-causing cell types in mouse and human non-ischemic fibrosis.

A. UMAP of mouse cellulome developed using the multiomic dataset generated in this study.
B. UMAP indicating Fibro-Cilp subcluster of fibroblasts and corresponding enrichment of transcripts corresponding to a fibrogenic signature (formed by the sum of average transcripts/cell for Col1a1, Col3a1, Col8a1, Tnc and Postn genes). Right-most panels show fibroblasts UMAPs with heatmaps of Cilp and Thbs4 gene transcripts in context of Saline and AngII treatment.
C. Immunostaining of AngII mouse hearts for THBS4. Nuclei and cell boundaries counterstained with DAPI and wheat germ agglutinin (WGA), respectively. Scale bar indicates 100 µm.
D. As for A, but using TAC dataset (GSE15588221).
E. As for B, but using TAC dataset (GSE15588221).
F. Immunostaining of TAC mouse hearts for THBS4. Nuclei and cell boundaries counterstained with DAPI and wheat germ agglutinin (WGA), respectively. Scale bar indicates 100 µm.
G. UMAP of human cellulome developed using the multiomic dataset generated in this study.
H. UMAP of human cellulome indicating Fibro-Cilp subcluster of fibroblasts and corresponding enrichment of transcripts corresponding to a fibrogenic signature (as defined above). Right-most panels indicate Thbs4 and Cilp gene transcript enrichment within the Fibro-Cilp subcluster.
I. Immunostaining of donor human heart for THBS4. Nuclei and cell boundaries counterstained with DAPI and wheat germ agglutinin (WGA), respectively. Scale bar indicates 100 µm.
J. Spatial transcriptomic mapping of remote regions of human cardiac cross sections highlighting the fibrogenic signature (as defined above) and THBS4 expression in control samples (from individual not undergone myocardial infarction) and remote zones of cardiac fibrosis (from individuals who have had myocardial infarction 20.

Figure 5

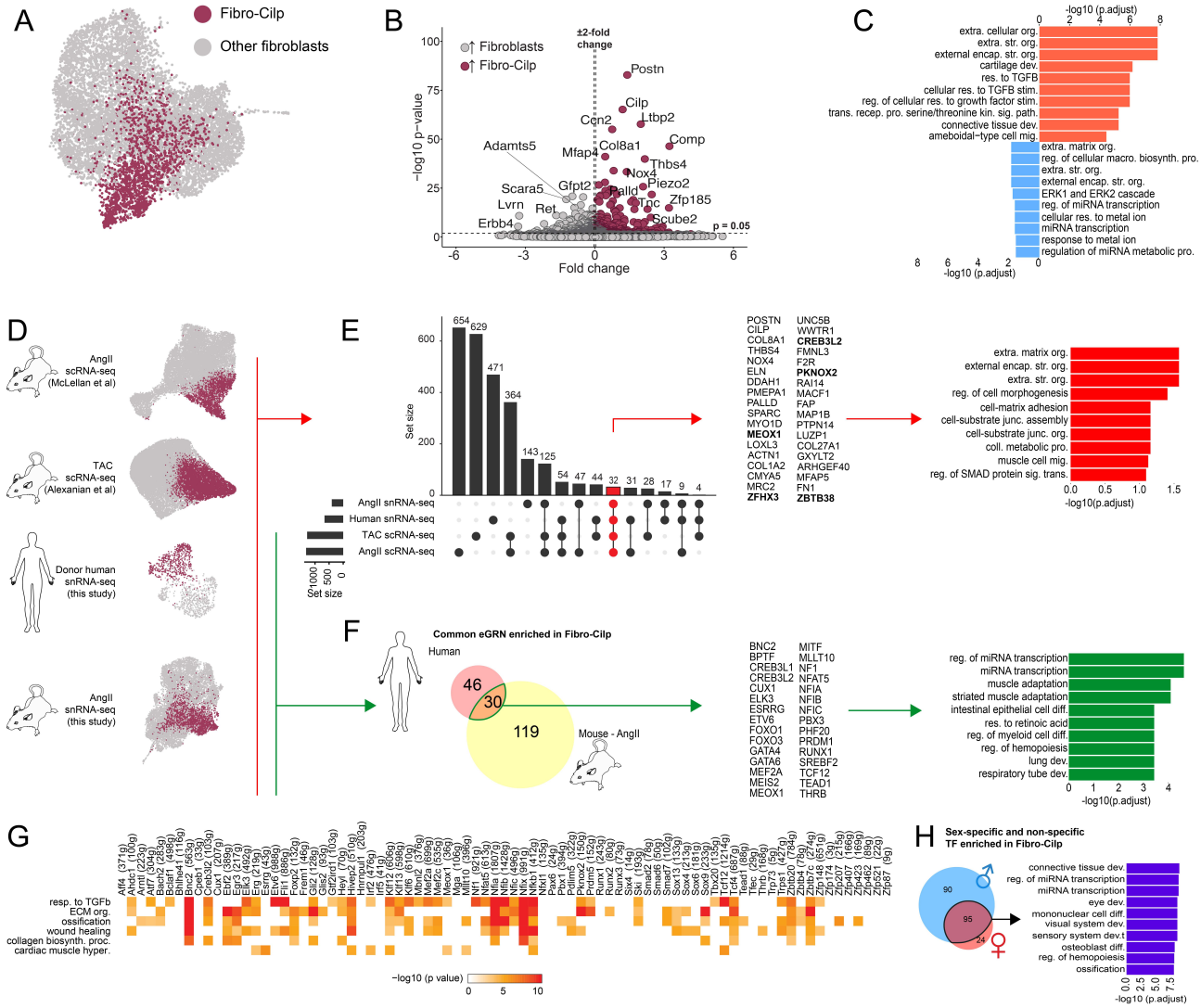

Figure 5. Similarity and differences in human and mouse on transcriptional level – integrating the Fibro-Cilp – Fibro-Thbs4 paradigm.

A. UMAP projection of cardiac fibroblasts from Saline and AngII mouse hearts used for subsequent analyses in B and C.
B. Volcano plot highlighting the up- and down-regulated genes in Fibro-Cilp cells when compared to other fibroblasts from AngII mouse hearts.
C. Top-10 GO terms corresponding to genes up- or down-regulated in Fibro-Cilp cells compared to other fibroblasts (orange and blue bars, respectively).
D. UMAPs of fibroblasts from mouse and human cardiac single-cell genomic datasets. Fibro-Cilp and other fibroblasts (non-Fibro-Cilp cells) shown in red and grey, respectively.
E. Overlap of genes enriched in Fibro-Cilp cells compared to other fibroblasts from the datasets shown in D. Upset plot (left-most panel) summarized entire gene sets from each datasets (horizontal bars) and genes that are present uniquely or in multiple datasets (vertical bars). Genes present in all datasets (indicated in red; 32 genes) and listed (middle panel; bolded genes indicated TFs). Top 10 GO terms corresponding to this list is shown in right-most panel.
F. Overlap in eRegulons identified as enriched in Fibro-Cilp cells vs other fibroblasts from mouse AngII and human donor datasets. Overlapping TF list and top GO terms corresponding to the TF genes are shown in middle and far-right panels, respectively.
G. Heat map of GO enrichment of TF target genes within eRegulons corresponding to fibrosis- and hypertrophy-related terms.
H. Overlap of lists of eRegulons enriched in Fibro-Cilp vs other fibroblasts from AngII mice independently determined for each sex.

Figure 6

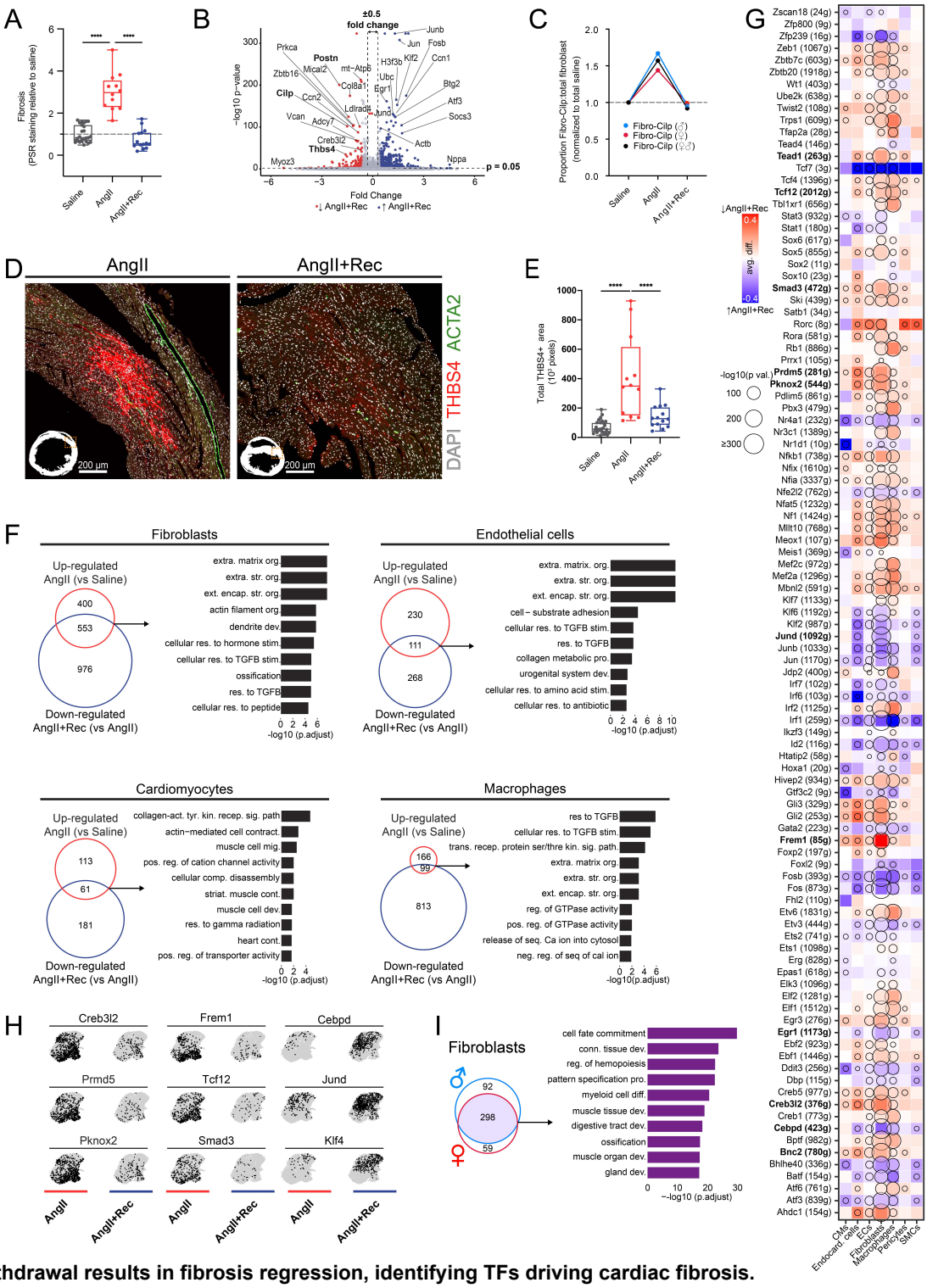

Figure 6. AngII withdrawal results in fibrosis regression, identifying TFs driving cardiac fibrosis.

A. Cardiac fibrosis in AngII and AngII+Rec mouse hearts relative to Saline mouse hearts determined by quantifying picrosirius red staining. $p < 0.01$ (one way ANOVA test).

B. Volcano plot of genes increased (blue) or decreased in gene expression in other fibroblasts from AngII+Rec mouse hearts compared to AngII mouse hearts. Note reduction in Thbs4 and Cilp gene expression.

C. Cellular abundances of Fibro-Cilp cells relative to total cells in the dataset corresponding to Saline, AngII and AngII+Rec groups. Proportion data is normalized to Saline group. Data specific to females (red dot/lines), males (blue dots/lines) or both female and males (black dots/lines) are shown.

D. Representative micrographs of THBS4 immunostaining within AngII and AngII+Rec mouse heart sections.

E. Change in THBS4 immunostaining in cardiac cross sections from AngII and AngII+Rec mouse hearts (N= 5-6 animals per group). $p < 0.01$ (one-way ANOVA test).

F. Overlap of genes up-regulated in major cardiac cells populations from AngII mouse hearts (relative to Saline) and those that are down-regulated in AngII+Rec mouse hearts (relatively to AngII). Venn diagrams summarize unique and common genes of within these gene sets. Bar plots summarize to GO terms corresponding to overlapping genes.

G. Heatmap/dot plot summarizing changes in eRegulon enrichment in cardiac cells types from AngII and AngII+Rec mouse hearts.

H. UMAPs displaying binarized eRegulons enrichment within fibroblasts from AngII or AngII+Rec mouse heart datasets. First two columns (Creb3l2, Prmd5, Pknox2, Frem1, Tcf12 and Smad3) show examples of TFs that are more active in AngII mouse heart fibroblasts (i.e. they are repressed in AngII+Rec mouse heart fibroblasts). Third column (Cepbd, Jund, Klf4) show examples of TFs that are repressed in AngII mouse hearts and are robustly activated in AngII+Rec mouse heart fibroblasts.

I. Summary of overlap eRegulons that are more highly enriched in cardiac fibroblasts in AngII+Rec mouse hearts compared AngII, from each sex. Venn diagram summarizes sex-specific and non-specific eRegulons. Bar plot summarizes top-10 GO terms related to TFs comprising overlapping eRegulons.

Figure 7

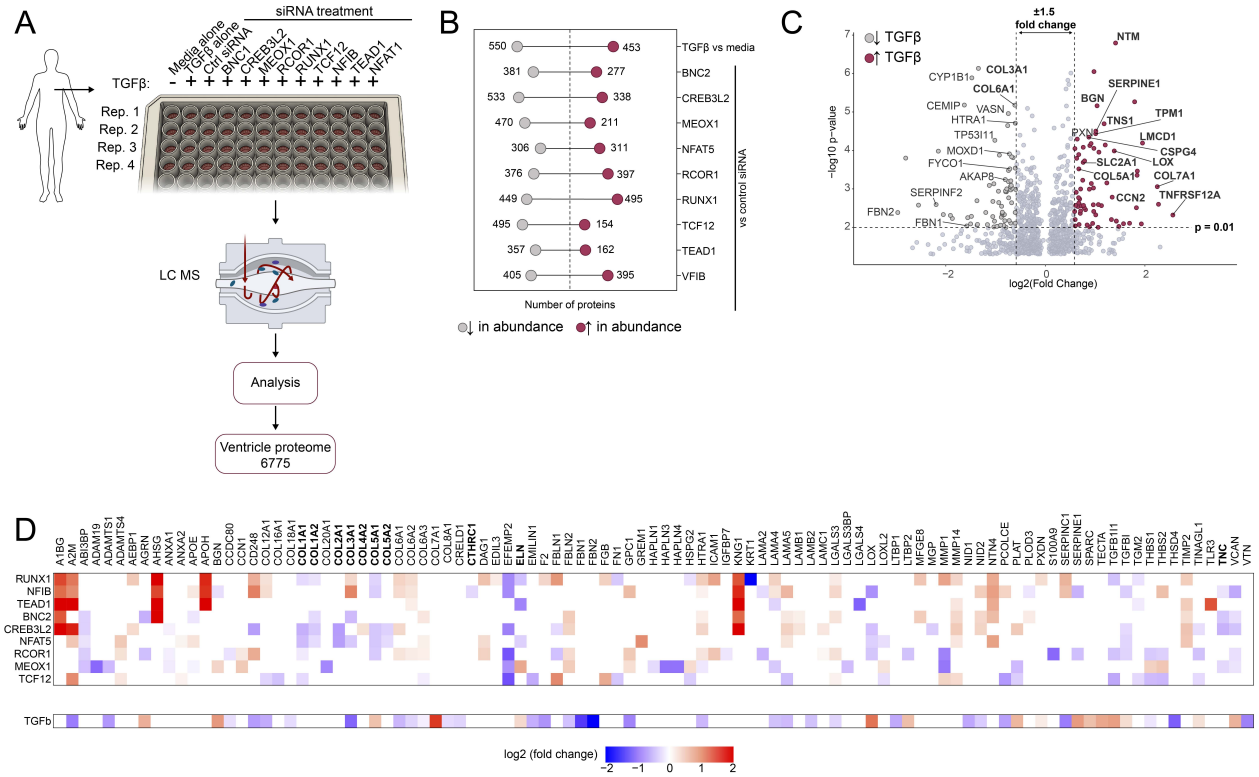

Figure 7. Proteome landscape of distinct roles of core TFs in ECM deposition and fibrosis.

A. Experimental schematic for proteomic evaluation of roles of core TFs identified in this study in ECM production in TGFβ-treated human primary cardiac ventricular fibroblasts. All conditions were tested in four replicates. After TGFβ treatment, cell cultures were analyzed by high-throughput mass spectroscopy-based proteomic profiling before subsequent informatics analyses.

B. Lollipop plots summarizing significant ($p<0.05$) differential expression of proteins in various comparisons indicated. TGFβ-treated cells were compared to media alone, whereas all TF siRNA-treated cells were compared to control siRNA-treated cells.

C. Volcano plot summarizing proteins increased or decreased in abundance after TGFβ treatment, compared to media alone control.

D. Heat map summarizing fold-increase or decrease in abundance of proteins in TF siRNA-treated cells compared to control siRNA-treated cells. Bottom panel also shows fold-increase or decrease in abundance of proteins in TGFβ-treated cells vs media alone control.

REFERENCES

1. Krstevski, C., Cohen, C. D., Dona, M. S. I. & Pinto, A. R. New perspectives of the cardiac cellular landscape: mapping cellular mediators of cardiac fibrosis using single-cell transcriptomics. *Biochem. Soc. Trans.* **48**, 2483–2493 (2020).

2. Pinto, A. R. *et al.* Revisiting cardiac cellular composition. *Circulation Research* **118**, 400–409 (2016).

3. Skelly, D. A. *et al.* Single-Cell Transcriptional Profiling Reveals Cellular Diversity and Intercommunication in the Mouse Heart. *Cell Rep.* **22**, 600–610 (2018).

4. Tucker, N. R. *et al.* Transcriptional and Cellular Diversity of the Human Heart. *Circulation* **142**, 466–482 (2020).

5. Koenig, A. L. *et al.* Single-cell transcriptomics reveals cell-type-specific diversification in human heart failure. *Nat. Cardiovasc. Res.* **1**, 263–280 (2022).

6. Litviňuková, M. *et al.* Cells of the adult human heart. *Nature* **588**, 466–472 (2020).

7. Forte, E. *et al.* Dynamic Interstitial Cell Response during Myocardial Infarction Predicts Resilience to Rupture in Genetically Diverse Mice. *Cell Rep.* **30**, 3149-3163.e6 (2020).

8. Kuppe, C. *et al.* Spatial multi-omic map of human myocardial infarction. *Nature* **608**, 766–777 (2022).

9. Peisker, F. *et al.* Mapping the cardiac vascular niche in heart failure. *Nat. Commun.* **13**, 3027 (2022).

10. McLellan, M. A. *et al.* High-Resolution Transcriptomic Profiling of the Heart During Chronic Stress Reveals Cellular Drivers of Cardiac Fibrosis and Hypertrophy. *Circulation* **142**, 1448–1463 (2020).

11. Pinto, A. R. *et al.* Revisiting Cardiac Cellular Composition. *Circ. Res.* **118**, 400–409 (2016).

12. González-Blas, C. B. *et al.* SCENIC+: single-cell multiomic inference of enhancers and gene regulatory networks. *Nat. Methods* **20**, 1355–1367 (2023).

13. Fang, F. *et al.* Early Growth Response 3 (Egr-3) Is Induced by Transforming Growth Factor-β and Regulates Fibrogenic Responses. *Am. J. Pathol.* **183**, 1197–1208 (2013).

14. Bourajjaj, M. *et al.* NFATc2 Is a Necessary Mediator of Calcineurin-dependent Cardiac Hypertrophy and Heart Failure*. *J. Biol. Chem.* **283**, 22295–22303 (2008).

15. Gaspar-Pereira, S. *et al.* The NF-κB Subunit c-Rel Stimulates Cardiac Hypertrophy and Fibrosis. *Am. J. Pathol.* **180**, 929–939 (2012).

16. Zhao, J., Hu, J., Zhang, R. & Deng, J. CEBPD REGULATES OXIDATIVE STRESS AND INFLAMMATORY RESPONSES IN HYPERTENSIVE CARDIAC REMODELING. *Shock* **60**, 713–723 (2023).

17. Penke, L. R. K. *et al.* KLF4 is a therapeutically tractable brake on fibroblast activation which promotes resolution of pulmonary fibrosis. *JCI Insight* **7**, e160688 (2022).

18. Alexanian, M. *et al.* A transcriptional switch governs fibroblast activation in heart disease. *Nature* **595**, 438–443 (2021).

19. Tham, Y. K. *et al.* Lipidomic Profiles of the Heart and Circulation in Response to Exercise versus Cardiac Pathology: A Resource of Potential Biomarkers and Drug Targets. *Cell Rep.* **24**, 2757–2772 (2018).

20. Kuppe, C. *et al.* Spatial multi-omic map of human myocardial infarction. *Nature* **608**, 766–777 (2022).

21. Alexanian, M. *et al.* A transcriptional switch governs fibroblast activation in heart disease. *Nature* **595**, 438–443 (2021).

22. Liu, X. *et al.* Lineage-specific regulatory changes in hypertrophic cardiomyopathy unraveled by single-nucleus RNA-seq and spatial transcriptomics. *Cell Discov.* **9**, 6 (2023).

23. Amrute, J. M. *et al.* Defining cardiac functional recovery in end-stage heart failure at single-cell resolution. *Nat. Cardiovasc. Res.* **2**, 399–416 (2023).

24. Morine, K. J. *et al.* Bone Morphogenetic Protein 9 Reduces Cardiac Fibrosis and Improves Cardiac Function in Heart Failure. *Circulation* **138**, 513–526 (2018).

25. Bobowski-Gerard, M. *et al.* Functional genomics uncovers the transcription factor BNC2 as required for myofibroblastic activation in fibrosis. *Nat. Commun.* **13**, 5324 (2022).

26. Hilfiker-Kleiner, D. *et al.* Lack of JunD Promotes Pressure Overload–Induced Apoptosis, Hypertrophic Growth, and Angiogenesis in the Heart. *Circulation* **112**, 1470–1477 (2005).

27. Malaab, M. *et al.* Antifibrotic factor KLF4 is repressed by the miR-10/TFAP2A/TBX5 axis in dermal fibroblasts: insights from twins discordant for systemic sclerosis. *Ann. Rheum. Dis.* **81**, 268–277 (2022).

28. Peisker, F. *et al.* Mapping the cardiac vascular niche in heart failure. *Nat. Commun.* **13**, 3027 (2022).

29. Vivar, R. *et al.* FoxO1 mediates TGF-beta1-dependent cardiac myofibroblast differentiation. *Biochim. Biophys. Acta (BBA) - Mol. Cell Res.* **1863**, 128–138 (2016).

30. Xie, Q. *et al.* High-Mobility Group A1 Promotes Cardiac Fibrosis by Upregulating FOXO1 in Fibroblasts. *Front. Cell Dev. Biol.* **9**, 666422 (2021).

31. Tamura, T., Said, S., Harris, J., Lu, W. & Gerdes, A. M. Reverse Remodeling of Cardiac Myocyte Hypertrophy in Hypertension and Failure by Targeting of the Renin-Angiotensin System. *Circulation* **102**, 253–259 (2000).

32. Ruppert, M. *et al.* Sex similarities and differences in the reverse and anti-remodeling effect of pressure unloading therapy in a rat model of aortic banding and debanding. *Am. J. Physiol.-Hear. Circ. Physiol.* **323**, H204–H222 (2022).

33. Boehm, M. *et al.* Delineating the molecular and histological events that govern right ventricular recovery using a novel mouse model of pulmonary artery de-banding. *Cardiovasc. Res.* **116**, 1700–1709 (2020).

34. Mclellan, M. A. *et al.* McLellan et al, transcriptomics of chronic cardiac stress High-resolution transcriptomic profiling of the heart during chronic stress reveals cellular drivers of cardiac fibrosis and hypertrophy. *Circulation* (2020) doi:10.1101/854026.

35. Farbehi, N. *et al.* Single-cell expression profiling reveals dynamic flux of cardiac stromal, vascular and immune cells in health and injury. *eLife* **8**, e43882 (2019).

36. Amrute, J. M. *et al.* Defining cardiac functional recovery in end-stage heart failure at single-cell resolution. *Nat. Cardiovasc. Res.* **2**, 399–416 (2023).

37. Yin, L. *et al.* Over-Expression of Inhibitor of Differentiation 2 Attenuates Post-Infarct Cardiac Fibrosis Through Inhibition of TGF-β1/Smad3/HIF-1α/IL-11 Signaling Pathway. *Front. Pharmacol.* **10**, 1349 (2019).

38. Wehrens, M. *et al.* Single-cell transcriptomics provides insights into hypertrophic cardiomyopathy. *Cell Rep.* **39**, 110809 (2022).

39. Remedios, C. G. D. *et al.* The Sydney Heart Bank: improving translational research while eliminating or reducing the use of animal models of human heart disease. *Biophys. Rev.* **9**, 431–441 (2017).

40. Zhu, C. *et al.* An ultra high-throughput method for single-cell joint analysis of open chromatin and transcriptome. *Nat. Struct. Mol. Biol.* **26**, 1063–1070 (2019).

41. Stuart, T., Srivastava, A., Madad, S., Lareau, C. A. & Satija, R. Single-cell chromatin state analysis with Signac. *Nat. Methods* **18**, 1333–1341 (2021).

42. Hao, Y. *et al.* Integrated analysis of multimodal single-cell data. *Cell* **184**, 3573-3587.e29 (2021).

43. Hafemeister, C. & Satija, R. Normalization and variance stabilization of single-cell RNA-seq data using regularized negative binomial regression. *Genome Biol.* **20**, 296 (2019).

44. McGinnis, C. S., Murrow, L. M. & Gartner, Z. J. DoubletFinder: Doublet Detection in Single-Cell RNA Sequencing Data Using Artificial Nearest Neighbors. *Cell Systems* **8**, 329-337.e4 (2019).

45. Farrugia, G. E. *et al.* A protocol for rapid and parallel isolation of myocytes and non-myocytes from multiple mouse hearts. *STAR Protoc.* **2**, 100866 (2021).

46. Skelly, D. A. *et al.* Single-Cell Transcriptional Profiling Reveals Cellular Diversity and Intercommunication in the Mouse Heart. *Cell Rep.* **22**, 600–610 (2018).

47. Aibar, S. *et al.* SCENIC: single-cell regulatory network inference and clustering. *Nat. Methods* **14**, 1083–1086 (2017).

48. González-Blas, C. B. *et al.* SCENIC+: single-cell multiomic inference of enhancers and gene regulatory networks. *Nat. Methods* **20**, 1355–1367 (2023).

49. Claridge, B. *et al.* Cardiomyocyte intercellular signaling increases oxidative stress and reprograms the global- and phospho-proteome of cardiac fibroblasts. *J. Extracell. Biol.* **2**, (2023).

50. Tham, Y. K. *et al.* Estrogen receptor alpha deficiency in cardiomyocytes reprograms the heart-derived extracellular vesicle proteome and induces obesity in female mice. *Nat. Cardiovasc. Res.* **2**, 268–289 (2023).

51. Cross, J., Rai, A., Fang, H., Claridge, B. & Greening, D. W. Rapid and in-depth proteomic profiling of small extracellular vesicles for ultralow samples. *PROTEOMICS* e2300211 (2023) doi:10.1002/pmic.202300211.